THE ASTRONOMICAL JOURNAL VOLUME 92, NUMBER 5 NOVEMBER 1986

MODELING PLUTO-CHARON MUTUAL ECLIPSE EVENTS. I. FIRST-ORDER MODELS

R. Scott Dunbar and Edward F. Tedesco
Jet Propulsion Laboratory, California Institute of Technology, Pasadena, California 91109
Received 29 May 1986; revised 7 August 1986

ABSTRACT

We present numerical and analytical models describing the light curves resulting from mutual events between close planetary binaries, with particular application to the Pluto-Charon system. These models are referred to as "first-order" models because they incorporate the effects of shadowing in such systems, in contrast to "zeroth-order" models, which do not include shadowing. The shadows cast between close binaries of similar size (as in the case of Pluto and Charon) can be treated as extensions of the eclipsing bodies themselves at small solar phase angles. Shadowing plays a major role in the morphology of mutual event light curves. The numerical approach is a straightforward, but computationally intensive, discrete-element integration. The analytical approach uses a conceptually simple model of three circular disks, representing the planet, satellite, and shadow, and computes the complex geometric relationship among these three disks to obtain the eclipse magnitude at each time step. The results of the two models agree to well within the expected light-curve measurement error. A preliminary model fit to the depths of five mutual eclipse events observed in 1985 and 1986 gives eclipse light-curve-derived estimates of the orbit radius $C = 16.5 \pm 0.5$ Pluto radii, the radius ratio $B_0 = 0.65 \pm 0.03$, and the Charon:Pluto albedo ratio $K = 0.55 \pm 0.15$. These model parameter estimates yield a system mass density of 1.6 ± 0.2 g/cm^3, and together with the absolute orbit radius give 2300 ± 100 km and 1500 ± 100 km for the diameters of Pluto and Charon, respectively. We estimate the geometric albedos of Pluto and Charon to be 0.6 and 0.3 (± 0.1), respectively, suggesting that limb darkening plays only a minor role in the mutual-event light curves. The model predicts that the current mutual eclipse event series will end by November 1990, with the last observable events occurring in mid-August of that year.

I. INTRODUCTION

Soon after the discovery of Pluto's satellite, Charon, it was recognized that the orientation of Charon's orbit would give rise to a series of mutual eclipse phenomena appearing during the 1980s (Andersson 1978). Such events can only occur near passages of the Sun through the plane of Charon's orbit, at about 124 yr intervals. Precise prediction of the onset of eclipse events was made difficult by the lack of resolved separation—position-angle observations for orbit determination prior to the use of speckle interferometry (Bonneau and Foy 1980; Tholen 1985). The observational difficulties are mainly due to the 0.9″ maximum apparent separation of Pluto and Charon. The first observations of Pluto-Charon mutual events were made in early 1985. These initial events and observations are described elsewhere (Binzel *et al.* 1985). We use the terms "eclipse" and "mutual event" to mean any of the possible phenomena which give rise to an event light curve. For example, transits and shadow transits (where Charon and/or its shadow pass wholly or partially in front of Pluto), or occultations and eclipses (where Charon passes behind Pluto and is obscured from view by Pluto, Pluto's shadow, or both).

Light curves of Pluto-Charon mutual events can be used to refine estimates of several dynamical and physical parameters of the system. These include improvement of the orbit of Charon, and determination of the diameters, masses, densities, and geometric albedos of Pluto and Charon, including detection of albedo differences between the two bodies and any large-scale albedo variation on the surface of Pluto. Since the uncertainties in nearly all of these parameters have been relatively large, our approach has been to choose a model which accurately portrays the main features of the eclipse events. It can then be used with observational data to reduce the uncertainties in some parameters sufficiently so that refinements of the model can be incorporated at a later time.

We present analytical and numerical models describing the light curves resulting from mutual events between close planetary binaries, with particular application to the Pluto-Charon system. These models are referred to as first-order models because they incorporate the effects of shadowing and albedo differences, in contrast to the previously published model of Mulholland and Binzel (1984) which assumed equal albedos and did not include shadowing. In this paper, we will differentiate between first-order and zeroth-order models only with respect to the inclusion of shadowing effects, while both types of models will include the effects of albedo differences, a relatively simple extension of the model. Unlike the eclipse events in more widely separated systems, such as the Galilean satellites of Jupiter, the shadows cast between close binaries of similar size (as in the case of Pluto and Charon) can be treated as extensions of the eclipsing bodies themselves for solar phase angles less than 10°. Wijesinghe and Tedesco (1979) demonstrated the importance of these extended shadows in their analytical model, which was developed to test the plausibility of eclipsing binary asteriods by contrasting the expected characteristics of their light curves with conventional rotational models. Shadowing plays a major role in the morphology of mutual-event light curves even at very small phase angles.

In the next section we briefly review the derivation of the necessary projection geometry for the mutual events. General modeling considerations are discussed in Sec. III. In Sec. IV we present a numerical model for simulating mutual-event light curves, and Sec. V describes the analytical model, based in part on the equations developed in Wijesinghe and Tedesco (1979). The results of these models are presented in

 0004-6256/86/051201-09$00.90

Sec. VI for a few selected cases, and the relative merits and future use of the two approaches is discussed in Sec. VII.

II. PROJECTION GEOMETRY OF ECLIPSE EVENTS

Simulation of an eclipse light curve depends on the relative sizes and separation of the bodies as well as the locations of the observer and the Sun. The projection of the observer-Sun-planet geometry onto the plane of the sky may be expressed in terms of the following five geometric quantities (see Fig. 1):

(1) the radius ratio $r(\text{secondary})/R(\text{primary}) = B_0$, i.e., all distances are normalized by R and all areas are normalized by the full cross-sectional area of the primary;

(2) the (normalized) orbit radius $C = \rho/R$, where ρ is the circular orbit radius;

(3) the solar phase angle α, which governs the shapes and areas of the illuminated surfaces and the extended shadows;

(4) the sub-Earth latitude angle ψ, defined with respect to the orbit plane of the satellite. This angle is the complement of the orbit aspect, usually defined as the angle between the orbit axis and the line-of-sight vector;

(5) the phase obliquity angle δ, defined as the angle between the major axis of the projected orbit ellipse and the projected illumination axis (i.e., the apparent planet-Sun line).

An alternative parameter which is often used is the "impact parameter" A_0, which in these normalized distance units is given by $A_0 = C \sin \psi$. The value of the impact parameter largely determines whether or not an eclipse is possible, and if so, whether it will be partial or total. No eclipse is possible for $A_0 > 1 + B_0$, partial eclipses occur for $1 - B_0 < A_0 < 1 + B_0$, and eclipses are total for $A_0 < 1 - B_0$. These relations are really exact only for the zero-phase case; when the extended shadows are included at nonzero phase angles, shadow-transit-type eclipses may still occur outside the $A_0 = 1 + B_0$ boundary for particular orbit/observation geometries.

The independent variable of the projected geometry is the orbital phase θ, which, if we assume a circular orbit, is very nearly the mean anomaly of the secondary measured from the position at some given epoch. The zero point of orbital phase is chosen to be the point on the orbit where the secondary object is at inferior conjunction and minimum apparent distance ($= A_0$) from the primary. Thus, for zero solar phase angle the time of zero orbital phase corresponds to the midpoint time of satellite transit, or "inferior eclipse," event minima (secondary in front of primary), while the time of 180° orbital phase corresponds to the midpoint of satellite occultation, or "superior eclipse," event minima (secondary behind primary). Due to the continuously changing observing geometry (solar phase, aspect, and obliquity), the mean anomaly difference between consecutive $\theta = 0°$ epochs is in general not equal to 360° ($\Delta T \approx$ orbit period), but the discrepancy is small and can be safely ignored for light-curve simulations of individual events, which cover only a small fraction of an orbit period, so long as the exact time of 0° (or 180°) orbital phase is computed rigorously from the observing geometry of date. As we shall see, in first-order eclipse models the time of minimum separation of the two bodies does not necessarily correspond to the observed time of the eclipse minimum or to the exact midpoint of an event's duration (measured from first to last contact). The shadow's size and orientation determine these timings, breaking the symmetry that is characteristic of zero-order (and zero solar phase) light curves.

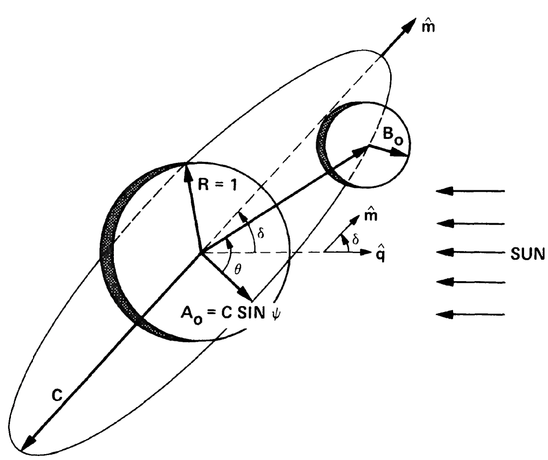

FIG. 1. Basic observing geometry of the Pluto-Charon eclipse system, showing the relationship of the derived angles α (solar phase), ψ (aspect), and δ (shadow obliquity) to the fundamental vectors $\hat{\mathbf{r}}$ (heliocentric Pluto position), $\hat{\mathbf{r}}$ (topocentric Pluto position), $\hat{\mathbf{h}}$ (Charon orbit pole), and $\hat{\mathbf{s}}$ (Plutocentric Charon position). The topocentric radius vector $\mathbf{r}$ is directed into the paper. The principal axis is defined to be $\hat{\mathbf{q}}$, the apparent illumination direction, and $\hat{\mathbf{m}}$ is the direction of the $\theta = 90°$ point on the apparent orbit ellipse.

Computation of the geometrical parameters α, ψ, δ, and θ involves a straightforward ephemeris calculation using the heliocentric orbit of the planet and the planetocentric orbit of the satellite as input. Care must be taken that all orbit elements and coordinates are referred to the same system. There are four fundamental unit vectors from which the model parameters can be calculated:

(1) $\hat{\mathbf{r}}$ = Sun-planet direction,
(2) $\hat{\mathbf{p}}$ = observer-planet (topocentric) direction,
(3) $\hat{\mathbf{h}}$ = satellite orbit axis direction,
(4) $\hat{\mathbf{s}}$ = planet-satellite direction of date.

The solar phase angle α is given by

$$\cos \alpha = \hat{\mathbf{r}} \cdot \hat{\mathbf{p}}, \tag{1}$$

and the sub-Earth latitude ψ is found from

$$\sin \psi = -\hat{\mathbf{p}} \cdot \hat{\mathbf{h}}. \tag{2}$$

The phase obliquity δ is somewhat more complicated because we first need to find the projection of the $\hat{\mathbf{r}}$ vector on the sky as seen by the observer. This projection is the illumination axis direction about which all phase effects (crescents and shadows) are symmetrical. Let this intermediate vector be $\hat{\mathbf{q}}$, defined to be directed toward the Sun and given by

$$\hat{\mathbf{q}} = \hat{\mathbf{p}} \times (\hat{\mathbf{r}} \times \hat{\mathbf{p}})/\sin \alpha, \tag{3}$$

where the factor of $\sin \alpha$ is required to normalize $\hat{\mathbf{q}}$. The projection of the satellite's major axis is

$$\hat{\mathbf{m}} = (\hat{\mathbf{p}} \times \hat{\mathbf{h}})/\cos \psi, \tag{4}$$

where again the $\cos \psi$ factor is for normalization. This projection vector is taken to point toward the $\theta = 90°$ point on the satellite's orbit. The phase obliquity δ is then given by $\cos \delta = \hat{\mathbf{q}} \cdot \hat{\mathbf{m}}$, which after simplification of the vector products via well-known identities becomes

$$\cos \delta = \hat{\mathbf{h}} \cdot (\hat{\mathbf{r}} \times \hat{\mathbf{p}})/(\sin \alpha \ \cos \psi). \tag{5}$$

The phase obliquity is taken to be measured counterclockwise from $\hat{\mathbf{q}}$ to $\hat{\mathbf{m}}$, thus determining the proper quadrant.

To determine the apparent orbital phase θ we must find the direction of zero orbital phase. This vector is found to be

$$\hat{\boldsymbol{\theta}}_0 = \hat{\mathbf{m}} \times \hat{\mathbf{h}} = -(\tan\psi)\hat{\mathbf{h}} - (\sec\psi)\hat{\mathbf{p}} \quad (6)$$

and the orbital phase θ of date is then found from

$$\cos\theta = \hat{\mathbf{s}}\cdot\hat{\boldsymbol{\theta}}_0. \quad (7)$$

Given θ for a particular date, the times of the nearest eclipse minima can be found to a good approximation from

$$t(\theta = 0°) = t(\text{date}) - \theta(P/360°),$$
$$t(\theta = 180°) = t(\text{date}) + 180° - \theta)(P/360°), \quad (8)$$

where P is the satellite's orbital period. The approximation can be improved by an iteration of the eclipse ephemeris on θ, using Eqs. (8) to compute a correction to the time and forcing θ to converge on 0° or 180°.

The relative radii B_0 and C are "free" parameters which are primarily constrained by eclipse light-curve observations and the best estimates of the orbit period and radius as well as "reasonable" estimates of the bulk density of the planet and its satellite.

III. GENERAL MODEL CONSIDERATIONS

The basic assumptions used by Wijesinghe and Tedesco (1979) in their binary asteriod eclipse model form a conceptually sound and simple starting point for the present first-order development of the Pluto-Charon light-curve problem. In that model the bodies were assumed to be spherical in circular orbits about their common center of mass, with a separation of only a few times the radius of the primary body. It was further assumed that both components have equal and uniform albedos with uniformly illuminated surface projections taken normal to the line of sight (no limb darkening). The principal feature of the model was the inclusion of the effect of the extended shadows of the eclipsing bodies at nonzero phase, and thus the Wijesinghe-Tedesco model was also a first-order model. The shadowing effect is of critical importance for accurately modeling the light curves of such systems, both in terms of the shape and depth of light-curve minima and the detailed timing of eclipse phenomena. The principal difference between the W-T model and the numerical and analytical approaches presented here lies in the ways that the extended shadows are handled.

The primary feature of the eclipse events which must be reproduced by the model is the effect of the extended shadows at nonzero solar phase. For a small relative orbit radius C, the shadow cast by the occulting object onto the eclipsed body at small phase angles is largely hidden by the occulting object's disk and thus appears as an extension of the occulting disk. Such an extension, if oriented toward the eclipsed body, effectively increases the occulting area of the disk, producing deeper minima. Another result is an orbital-phase shift of the actual minimum away from the expected $\theta = 0°$ and 180° (as defined here), which is due to the offset of the centroid of the "shadow + disk" effective occulting area from the projected center of the disk alone. This offset is dependent on both the solar phase angle and the orbital radius of the satellite. Larger phase angles and orbit radii increase the projected length of the shadow cylinder, and thus the projected area of obscuration.

A secondary effect is that of "gibbousness" of both bodies when $\alpha \neq 0$. Gibbousness is the decrease in the illuminated areas of both bodies at nonzero phase, and depends solely on the solar phase angle. This may be accounted for in two ways: (1) the uneclipsed intensity of the two bodies, which is the brightness to which the eclipse minima are referred, must be adjusted for this phase-dependent effect, and (2) the eclipse of the "dark crescent" of the eclipsed body does not contribute to the light variation, while that of the eclipsing body is part of the total occulting (shadow + disk) area. At the small phase angles ($<2°$) that occur in the Pluto-Charon case, however, gibbousness is insignificant, contributing much less than a 0.1% reduction in the illuminated areas of the bodies (i.e., <0.001 mag), a considerably smaller effect than shadowing.

The next two sections describe the numerical and analytical first-order models which have been developed to analyze the observational eclipse data expected during the Pluto-Charon mutual-event series. We have chosen to pursue both approaches simultaneously, because each has certain advantages over the other, and because the development of two independent models provides important internal consistency checks.

IV. THE NUMERICAL MODEL

The numerical approach we have adopted consists of an integration over the illuminated surface of the eclipsed body. If the eclipsed body has an albedo distribution $k(x,y)$, the total observed intensity at a given time of an event is proportional to

$$L = \int k(x,y)\ dx\ dy, \quad (9)$$

where the integral is taken to be nonzero only on the illuminated surface. The change in the observed intensity of the system due to the eclipse is

$$\Delta m = 2.5\ \log\frac{L + k(\mathrm{t})A(\text{transit})}{A(\text{total})}, \quad (10)$$

where A(transit) is the illuminated surface of the eclipsing body and $A(\text{total}) = k(\mathrm{t})A(\text{transit}) + k(\mathrm{e})A(\text{eclipsed})$ is the total uneclipsed area of the two bodies [weighted by their mean albedos k(t) and k(e)]. To perform the surface integration in Eq. (9), the boundary of the illuminated surface of the eclipsed body must be properly defined.

We have chosen a Cartesian coordinate system with the origin at the center of the planet, in which the x axis is aligned with the major axis of the projected satellite orbit ellipse, positive toward the $\theta = 90°$ orbital-phase point. The y axis points to the projected orbit "north," and the z axis points along the observer's line of sight. Three vectors necessary to the solution of the problem can then be constructed (see Fig. 2):

(1) $\mathbf{r}$ = the position vector of the point (x,y,z) on the surface of the eclipsed body;

(2) $\mathbf{r}_0$ = the position vector of the satellite with respect to the planet;

(3) $\mathbf{r}_s$ = the position vector of the shadow of the eclipsing body.

The satellite vector $\mathbf{r}_0$ is given by

$$\mathbf{r}_0 = C[\sin\theta,\ \cos\theta\sin\psi,\ \cos\theta\ \cos\psi], \quad (11)$$

and the shadow vector $\mathbf{r}_s$ is

$$\mathbf{r}_s = C[\sin\alpha\ \cos\delta,\ \sin\alpha\ \sin\delta,\ \cos\alpha], \quad (12)$$

where the orbital phase θ, solar phase angle α, and shadow obliquity δ have been determined as in Sec. II, and C is the orbit radius in planetary radii. The vector $\mathbf{r}$ depends on the type of event considered; for satellite transit (inferior) events,

$$\mathbf{r} = [x,y,z],\ z^2 = 1 - x^2 - y^2, \quad (13)$$

and for satellite occultation (superior) events,

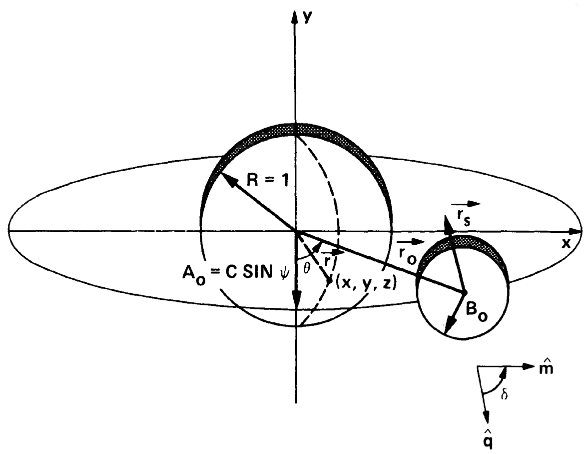

FIG. 2. Geometry for the numerical eclipse light-curve model. The x axis is taken along the major axis of the apparent orbit ellipse, and the z axis is out of the paper (the observer's line of sight). The **r** vector defines the point on the surface of Pluto to be tested for occultation, **r** is the radius vector of Charon, and **s** defines the extent and direction of the shadow cylinder axis. The integration grid is centered on Pluto for inferior events. Charon and the vectors **r** and **s** originate at Charon, while the origin of $\mathbf{r}_s$ is at Pluto.

$$\mathbf{r} = [x,y,z], \; z^2 = B_0^2 - x^2 - y^2. \tag{14}$$

We can now define the illuminated area of integration for L in terms of these vectors by the following constraints on the point (x,y) as observed in the plane of the sky:

$$\text{Constraint (1)}: x^2 + y^2 < 1 \quad \text{(inferior events)}$$
$$< B_0^2 \quad \text{(superior events)}, \tag{15}$$

$$\text{Constraint (2)}: (x - x_0)^2 + (y - y_0)^2 > B_0^2 \quad \text{(inferior)}$$
$$> 1 \quad \text{(superior)}, \tag{16}$$

$$\text{Constraint (3)}: |\mathbf{r} - \mathbf{r}_0 - S\mathbf{r}_s| > B_0 \quad \text{(inferior)}$$
$$> 1 \quad \text{(superior)}, \tag{17}$$

where S is the direction cosine of **r** with respect to the vector $(\mathbf{r} - \mathbf{r}_0)$:

$$S = \mathbf{r}_s \cdot (\mathbf{r} - \mathbf{r}_0)/C^2. \tag{18}$$

Constraint (1) simply says that the point (x,y) must lie on the eclipsed body, constraint (2) says that (x,y) must lie outside the disk of the eclipsing body, and constraint (3) says that (x,y) must also lie outside the shadow cone of the eclipsing body. If the point (x,y) satisfies all of these constraints, it must lie on the illuminated surface and therefore contributes to the integral in Eq. (10).

In practice, the calculation of L is performed on a grid of discrete elements of resolution size R covering an area of 2×2 planetary radii. For each grid element the constraints are tested, and if passed, the area of the element (R^2) is added to the total, weighted by the albedo. At this preliminary stage of the model we are using only a mean albedo for each body, normalized to the albedo of the planet. The calculation is sufficiently general, however, to allow weighting of each element's intensity for limb darkening as well as for nonuniform albedo distribution $k(x,y)$. One unfortunate consequence of this numerical approach (which is natural for numerical integration in general) is the number of calculations which must be performed on 20 000–40 000 grid elements to produce a single point on a light curve. At this early predictive stage, prior to nearly all of the expected observations, such a slow calculation of model light curves effectively precludes a comprehensive survey of the mutual-event phenomenology to be expected. For this reason we have chosen to pursue the analytical approach, described in the next section.

V. THE ANALYTICAL MODEL

It was expected that an analytical model would be sufficiently accurate for the initial analysis of observations while being very fast computationally, and might give better insight into the problem than the original Wijesinghe-Tedesco model, which used an "equivalent circle" approximation to account for shadowing and a division of the problem into four "zones." That model suffered from discontinuities near the zone boundaries, and inaccurately predicted the first and last contacts in events where shadowing was involved. We then tried a variation of the Wijesinghe-Tedesco model, in which the occulting disk was approximated by an equivalent ellipse. In this model, the zone specification was discarded and thus eliminated the discontinuity problem, but the calculation of the ellipse-on-circle overlap was rather slowly convergent and sometimes unstable, so that good agreement with the numerical model was rarely achieved.

At the suggestion of M. Buie (personal communication) we decided to try a three-circle approximation in place of the equivalent circle method of the W-T model. The result of this suggestion is the algorithm described below, in which the projections of the two bodies and the shadow are treated as overlapping circular disks. This three-circle approximation is extremely fast, continuous, and rigorously exact, with none of the problems of the previous models. Moreover, as will be shown, the three-circle model gives uniformly excellent agreement with the numerical model, to well within the expected measurement error of the light-curve observations.

The analytical eclipse light-curve model with the three-circle approximation uses the same projection equations (with corrections, see Appendix) as the W-T model calculation. The coordinates are referred to a system where the principal ("x") axis is the projected planet-Sun line, called the illumination axis, and the "y" axis is orthogonal to the illumination axis and directed in the usual right-handed sense. The key geometric variables for the problem are depicted in Fig. 3; these are the projected radius vectors **L** and **L**′ and position angles φ and φ' and the shadow offset h. The calculation of these quantities from the event geometry parameters derived in Sec. II is not given here; the reader is referred to the Appendix.

The interpretation of the projection vectors **L** and **L**′ depends on the type of event. For inferior events (Charon in front of Pluto) these vectors are directed from the center of the planet disk (the origin of the coordinate system) to the centers of the satellite and shadow disks, respectively; the shadow offset h associated with the satellite is the vector difference of the position vectors. For superior events, the planet-satellite vector **L** still connects the centers of the respective disks, but the shadow vector **L**′ has its origin at the planet's offset shadow center and is directed toward the center of the satellite's disk. The superior-event case is essentially equivalent to a translation of the origin of the coordinate system to the center of the satellite disk. Such a translation is not explicitly performed in the calculation; the three-circle algorithm is identical for both the inferior- and superior-

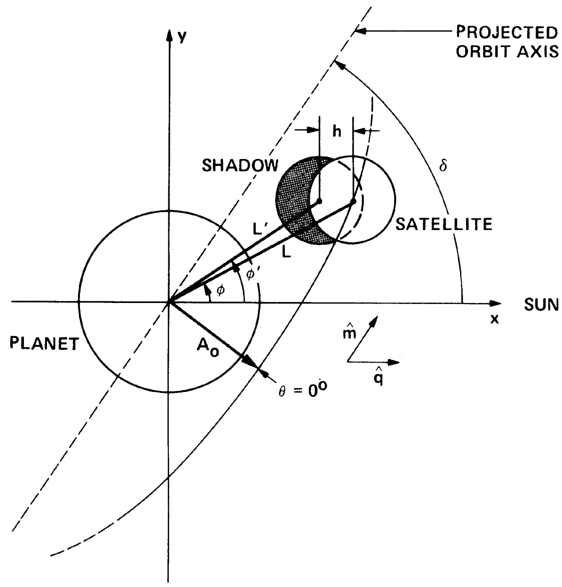

FIG. 3. Geometry for the analytical eclipse model. The x axis is the illumination axis, as in Fig. 1. The model treats the planet, satellite, and shadow as flat circular disks of radius 1, B_0, and B_0, respectively (inferior events). The relative positions of the disks are defined by the separation/position-angle coordinates (L/φ) (planet-satellite), (L',φ') (planet-shadow), and $(h,0)$ (satellite-shadow). For superior events, the roles of the planet and satellite are reversed, as in the numerical model.

event cases, the only difference being the assignment of the radii of the eclipsing and eclipsed bodies and the shadow.

The assumption that the disks are uniformly illuminated implies that the fractional change in the total intensity $\Delta I/I_0$ of the two bodies is proportional to the ratio of the area of overlap to the total uneclipsed area of the disks. We have explicitly introduced the (satellite:planet) albedo ratio K into the model formulas. The contribution of each body to the total brightness of the system is taken to be the product of its illuminated area and albedo. The effect of gibbousness, though small, is partially accounted for by the inclusion of a $\cos^2(\alpha/2)$ factor in the uneclipsed area ("intensity") I_0. Unlike the original W-T model, we have not attempted to include the elliptical shape of the gibbous hemispheres of the bodies, because of the small phase angles in the Pluto problem. Hence the total uneclipsed intensity is proportional to

$$I_0 \approx \pi(1+KB_0^2)\cos^2(\alpha/2). \tag{19}$$

The intensity change ΔI, which is proportional to the overlap area ΔA, also depends on the albedo of the eclipsed body. For superior events the fractional change in intensity is

$$\Delta I/I_0 = K\ \Delta A/[\pi(1+KB_0^2)\cos^2(\alpha/2)], \tag{20}$$

while for inferior events we have

$$\Delta I/I_0 = \Delta A/[\pi(1+KB_0^2)\cos^2(\alpha/2)]. \tag{21}$$

For $K<1$, we expect the inferior events to have deeper minima than superior events. For $K=1$, there should be no difference between the depths. The intensity variation in magnitudes is given by

$$\Delta m = 2.5\ \log[1-(\Delta I/I_0)]. \tag{22}$$

The key computation is thus the total area of intersection of the planet, satellite, and shadow disks, ΔA. In order to describe the three-circle algorithm, let us define the areas A_{12}, A_{13}, A_{23}, and A_{123}, where the subscript 1 is the eclipsed body, 2 denotes the eclipsing body, and 3 the shadow disk associated with body 2. The A_{ij} are the two-circle intersection areas, which are given by the formulas

$$A_{ij} = R_i^2 v_{ij} - d_{ij}R_i\ \sin v_{ij} + R_j^2 u_{ij}, \tag{23}$$

$$\cos v_{ij} = (R_i^2 - R_j^2 + d_{ij}^2)/2d_{ij}R_i, \tag{24}$$

$$\cos u_{ij} = (R_j^2 - R_i^2 + d_{ij}^2)/2d_{ij}R_j, \tag{25}$$

where d_{ij} is the distance between the centers. The area A_{123} is the triple intersection of all three disks, if present. In the present case of extended (but not independent) shadows, the area A_{23} always exists, while the areas A_{12} and A_{13} may or may not exist. The radii may have values of either 1 or B_0, with $R_2=R_3$, and the distances d are $d_{12}=L$, $d_{13}=L'$, and $d_{23}=h$.

To start the algorithm for a particular point in the light curve, the areas A_{ij} are computed. A test based on the value of either Eq. (24) or Eq. (25) determines whether the overlap is zero, partial or total; for $\cos u_{ij}>1$, $A=0$, and for $\cos u_{ij}<-1$, $A_{ij}=\pi B_0^2$. Another test is computed to decide whether the shadow intersection points I_1 and I_2 lie within circle 1. This leads to the following cases (see Fig. 4).

Case 1. Neither I_1 nor I_2 in circle 1:

$$\Delta A = A_{12}, \quad \text{if } L<L',$$

$$\Delta A = A_{13}, \quad \text{if } L'<L,$$

Case 2. Both I_1 and I_2 in circle 1:

$$\Delta A = \pi R_2^2 - A_{23} + A_{ij},\ j=2,\ \text{if } L<L'$$
$$j=3,\ \text{if } L'<L,$$

Case 3. Only one of I_1 or I_2 in circle 1:

$$\Delta A = A_{12} + A_{13} - A_{123}.$$

These cases connect smoothly as the relative geometry of the three disks changes. Case 3 is the most general and frequent situation encountered, especially for near-zero phase angle (small h) events, and is the case where the triple intersection A_{123} of the three disks comes into play.

The general calculation of A_{123} is straightforward, depending only on the position angles φ and φ', the radii of the three circles, and their mutual separations d_{ij}. The area is divided into a triangle bounded by the chords drawn between each of the points of intersection and the remaining three (sector-triangle) areas. The angles subtended at the centers of the three disks by the arcs which bound A_{123} are given by

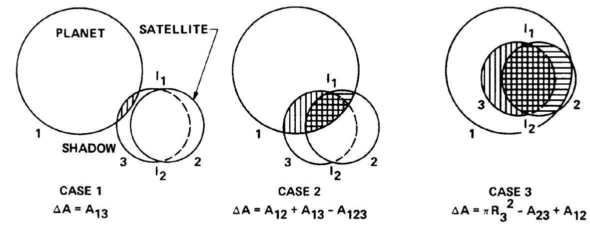

FIG. 4. 3-circle overlap algorithm. Three cases are possible: (a) Neither intersection point (I_1 or I_2) of disks 2 and 3 is contained within disk 1, effectively giving only 2-circle overlap; (b) One intersection point in disk 1, requiring computation of the triple overlap region A_{123}; (c) Both intersection points in disk 1, giving a combination of total overlap, and 2-circle overlap with disk 1, from which the overlap A_{23} must be subtracted.

$$w_1 = v_{12} + v_{13} - |\varphi - \varphi'|,$$
$$w_2 = u_{12} + u_{23} - \varphi,$$
$$w_3 = u_{13} + u_{23} + \varphi' - \pi, \tag{26}$$

where the u_{ij} and v_{ij} are the associated two-circle angles computed via Eqs. (24) and (25). The sides of the inscribed triangle are computed from

$$a_i = 2R_i \sin(w_i/2), \quad (i = 1,...,3), \tag{27}$$

and the areas of the (sector-triangle) segments are found from

$$S_i = R_i^2(w_i - \sin w_i)/2. \tag{28}$$

The area T of the triangle is computed from the lengths of the three sides by

$$T^2 = p(p - a_1)(p - a_2)(p - a_3), \tag{29}$$

where $p = (a_1 + a_2 + a_3)/2$. All four segments are then added to give the total area $A_{123} = T + S_1 + S_2 + S_3$.

In spite of the relative complexity of the calculation, this algorithm is more than 100 times faster than the discrete-element numerical algorithm because the entire set of calculations is performed only once per time step. This speed advantage permits a wider survey of mutual-event phenomenology, and will become useful in the early analysis of observational data to optimize rapidly the mean values of system parameters.

VI. MODEL LIGHT CURVES AND PREDICTIONS

a) Initial Model Parameters

As a basis for calculating the geometrical parameters φ, ψ, and δ, we began with the "adopted" Charon orbit of Tholen (1985). This orbit was determined primarily from speckle observations, but includes a $+1.0°$ correction applied to the true anomaly at the epoch in order to match the time of the 20 February 1985 observed light-curve minimum. In addition, on the basis of preliminary results from two events in early 1986, we have applied a correction of $-1.0°$ to the longitude of the ascending node. Thus eclipse light-curve observations have already played a role in the correction of Charon's orbit.

The remaining parameters, the ratios B_0, C, and K, have been estimated from the observations by adjustment of their values to achieve the best fit to the observed eclipse depths. Using the adopted orbit in Table I and the observations from the five events listed in Table II, the values $B_0 = 0.65$, $C = 16.50$, and $K = 0.55$ have been deduced. This model parametrization fits the observed event depths for all five events very well. Several other models were tried, most with unsatisfactory results. One model which fits the 1985 events very well ($\Omega = 223.7°$, $B_0 = 0.45$, $C = 12.15$, $K = 0.75$), and which was our initial baseline model until the 1986 observations were obtained, underestimates the depths of the 1986 events by as much as 0.1 mag. Another model ($\Omega = 222.8°$, $B_0 = 0.56$, $C = 15.00$, $K = 0.55$) fits the preliminary 1986 event depths well, but overestimates the 1985 depths by about 0.05 mag (which is significant when compared to the observed depths).

TABLE I. Adopted model and orbit parameters derived from 1985–1986 eclipse observations.

Parameter	Adopted value	Notes
Orbit radius	19130 ± 460 km	from Tholen (1985)
Orbit period	6.38723 days	"
Inclination	94.3 ± 1.5 deg	"
True anomaly	79.6 ± 1.9 deg	"
Epoch	2445000.5 JED	"
Ascending node	222.7 ± 1.0 deg	Eclipse model fit
Charon radius (B_0)	0.65 ± 0.03 Pl.R.	"
Orbit radius (C)	16.50 ± 0.5 Pl.R.	"
Albedo ratio (K)	0.55 ± 0.15	"

TABLE II. Preliminary model fit to observed mutual eclipse events.

Event time (UT)	Observed depth (mag)	Model prediction	Residual (O − C)	Notes
1985 Jan 16.467	0.04 ± 0.01	0.032	$+0.008$	a
1985 Feb 17.385	0.031 ± 0.005	0.045	-0.014	a
1985 Feb 20.585	0.024 ± 0.004	0.024	0.000	a
1986 Mar 20.382	0.25 ± 0.01	0.248	$+0.002$	b
1986 Apr 5.354	0.12 ± 0.01	0.117	$+0.003$	c
	rms residual = ± 0.007 mag			

[a] From Binzel *et al.* (1985).
[b] Observer Tedesco, Kitt Peak National Observatory, 1.3 m reflector.
[c] Observers Tedesco and Nelson, Kitt Peak National Observatory, 1.3 m reflector.

We have estimated the uncertainties in the parameters B_0, C and K by computing the variation of the model eclipse depth Δm for each of the events in Table II. The partials of Δm with respect to each of the parameters were computed from the model for each event, centered on the adopted model. These partials were then used to scale the estimated uncertainties in the observed depths into estimates of the parameter errors, giving an upper limit on the variation of each parameter (assuming the others are held fixed). The averages over the five events were then computed to obtain the mean uncertainties $\Delta B_0 = \pm 0.03$, $\Delta C = \pm 0.5$, and $\Delta K = \pm 0.15$.

The adopted model is the best fit obtained for both years' events, and therefore is much more tightly constrained than the model based on the 1985 events alone. It is important to note that the 1986 events by themselves place more severe restrictions on the model than do the earlier events, and so should receive greater weight in determining a model. The model should be regarded as preliminary, pending the full analysis of the 1986 events, and is not necessarily a unique solution. The fit to the observations is very good, with an rms error of 0.007 mag, and the detailed fit to the 20 March and 5 April light-curve data is excellent. The full analysis of the observations of these and other events and the determination of model parameters will be discussed in a future paper.

It should be kept in mind that these models are first-order models, treating the main features of the problem, but excluding limb-darkening and surface-albedo variations. In particular, if limb darkening is significant, it would be most evident in the 1985 eclipse events, which were shallow, limb-grazing events. On the other hand, limb darkening is not as important in the 1986 events because the degree of areal overlap is much greater, dominating any limb effects. Although a full treatment of limb darkening has not yet been developed for the present model, we can estimate the importance of limb darkening on the basis of the observed apparent magnitudes, the known observing geometry, and the model parameter $K = 0.55 \pm 0.15$. From this analysis we estimate the individual geometric albedos to be 0.6 for Pluto and 0.3 for Charon (with uncertainties of about ± 0.10 for each). Buratti (1984) has noted that for albedos up to about 0.6, limb darkening should still be a minor effect (though it is important to note that the estimate derived for Pluto lies nearly on this boundary). Limb-darkening effects will be negligible for superior events, given the estimated Charon albedo. Therefore, we may consider the adopted model, with no limb darkening, to give a good approximation to the parameters of the Pluto-Charon system.

This model implies several features about the Pluto-Charon system. It requires the albedo ratio to be quite low, $K = 0.55$, to fit the observations. This implies that the surface of Charon is markedly different from that of Pluto. The most striking feature implied is the large size of Charon relative to Pluto.

The average density of the system can be estimated from the model using the relation

$$\rho_{\rm ave} = \frac{3\pi C^3}{GP^2(1+B_0^3)}, \tag{30}$$

where G is the universal gravitation constant (more conveniently expressed as 498.1 cm^3/day^2), and P is the orbital period of Charon, 6.38723 days. Note that no absolute linear dimensional parameters are required to calculate the density. Using the model values of B_0 and C and their estimated uncertainties, $\rho_{\rm ave} = 1.6 \pm 0.2$ g/cm^3. This value for the density can be contrasted with the value of 0.75 g/cm derived from the early baseline model, which fit only the 1985 observations and which places unusual constraints on the composition. The value from the adopted model is consistent with the densities of outer solar system satellites.

If we introduce the orbit radius of $19\,130 \pm 460$ km, the model yields diameters of 2300 ± 100 km for Pluto and 1500 ± 100 km for Charon. The Charon diameter is consistent with the lower limit of 1200 km given by Walker's (1980) chord from a stellar occultation. The Pluto diameter is much smaller than the estimates derived from speckle observations [e.g., Bonneau and Foy 1980 (4000 km); Hege *et al.* 1982 (3000 ± 400 km)], but it is consistent with the radiometric observations of Lebofsky *et al.* (1982) which placed an upper limit of 2600 km on the diameter. All of these results (including the present one) are of course model dependent, but the eclipse light-curve data continue to place tighter constraints on the model as each event is observed.

b) Model Predictions

Figure 5 illustrates the predictions of the adopted model for three pairs of inferior and superior events in 1987. We have computed the full duration for each of the events using both the analytical and numerical models. The events were selected for the following reasons:

(1) The February events are at nearly maximum solar phase angle and the smallest separation distance for the entire year;

(2) The April events are at minimum solar phase angle (nearly at opposition);

(3) The July events are at maximum solar phase with the shadow pointing toward the eclipsed body, giving maximum shadowing effects.

Each first-order light curve is accompanied by the equivalent zero-order model light curve (plotted as a dashed curve), which was computed by setting $\alpha = 0°$ in the analytical model. The difference between the curves graphically shows the contribution of the shadow to the light curve. The event time (in hours) on the abscissa of each light curve is measured relative to the computed UT of 0° or 180° orbital phase. These examples clearly demonstrate the critical importance of shadowing effects in Pluto-Charon eclipse light

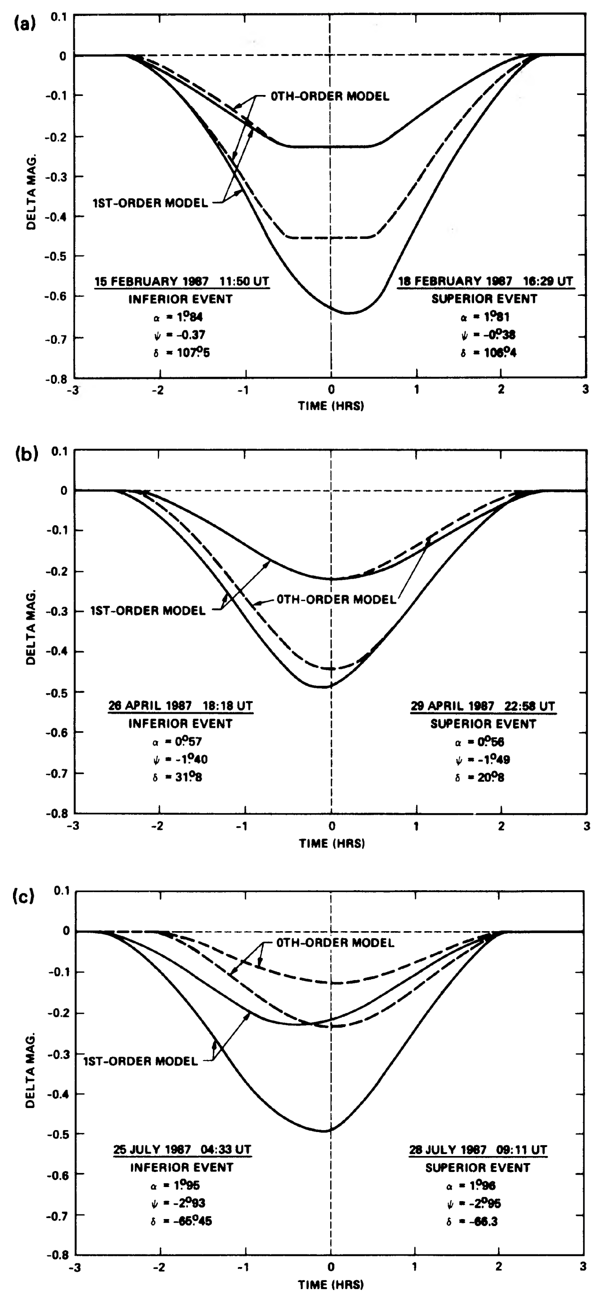

FIG. 5. Eclipse model light curves for adjacent pairs of (a) pre-opposition, (b) opposition, and (c) post-opposition inferior and superior events in 1987, based on the adopted model and orbit parameters (Table I). The dashed curves represent the results of the zero-order model, which neglects shadowing (but includes the albedo ratio $K = 0.55$), and the solid curves are the results of the adopted first-order model discussed in this paper. The differences between the depths of inferior and superior eclipses in each pair are mainly due to the albedo differences found from the model fit.

curves, and why it is necessary that these effects be accurately modeled. The numerical and analytical models give results which agree to better than 0.005 mag for the depths of the events.

The 1987 events are considerably deeper, with greater contributions from shadowing, than the events in 1985 and 1986. In 1985, eclipse events occurred only in the early pre-opposition period (up to March of that year) and were shallow, basically grazing eclipses with no shadowing. Post-opposition eclipses in 1985 were precluded by the separation distance of the two bodies, which was also too large to support shadow-transit events. The model and observations show that the 1986 eclipse events were considerably deeper in the pre-opposition period. In spite of the increasing aspect (separation), the post-opposition events should also be quite deep (about 0.2 mag) largely due to shadowing effects, which contribute as much as 0.15 mag to the eclipse depths in July and August 1986.

It is significant that the zero-order model predicts a classical flat-bottomed total "disk-only" inferior eclipse in February 1987, while the first-order models show no such effect, because the shadow is not yet completely contained in the planet's disk. The first and last contacts for this light curve are roughly symmetric about the 0° orbital-phase time, but the time of the minimum is skewed "late" due to the orientation of the shadow. The adjacent superior event of 18 February does, however, exhibit the "total" effect because of Charon's smaller size. In the 26 April event, the light curve is quite symmetric about the actual minimum because the shadow is leading almost directly ahead of the satellite disk along the transit chord. The minimum is less sharp than in the February event, and is shifted "early" because the disk + shadow centroid is offset ahead of the disk center. In the 25 July event the shadow contact occurs about 35 min ahead of the disk contact. The following superior event of 28 July also shows significant shadowing effects, with the minimum also skewed early. These light curves are considerably different from those expected from a zero-order model; shadowing is the dominant contributor to the features of this event.

The present model predicts the onset of flat-bottomed total eclipse minima for superior events starting in December 1986 through early April 1987, and for inferior events (with both the satellite disk and the entire shadow completely contained within the planet's disk) starting in 1988. Due to the large relative radius of Charon, the duration of the total phase of these events is brief, no more than about 40 min out of event durations of more than 5 hr.

The depth of the minimum at totality varies with the size of the shadow, and is thus controlled by the solar phase angle. In the limit of zero phase angle, corresponding to the nonshadow case, one expects total eclipse depths to be given by

$$\Delta m = 2.5 \log \left[1 - B_0^2/(1 + KB_0^2) \right], \qquad (31)$$

where for the adopted set of light-curve parameters, $\Delta m(\alpha = 0°) = -0.456$ mag for inferior events and -0.227 mag for superior events. When shadowing is included at nonzero phase, the depth is increased significantly for inferior events; at the maximum solar phase angle for Pluto, $a \approx 1.96°$, the depth becomes -0.788 mag. Shadowing can increase the depths of Pluto-Charon eclipses by about 0.1–0.3 mag, even at such small phase angles.

After the 1988 series, during which (using the orbit in Table I) the Earth crosses the Charon orbit plane three times (23 November 1987, 1 June 1988, and 19 September 1988), the overall eclipse cycle begins to reverse. From January to mid-April of 1990, the events will consist of shadow-only events because the separation is too large for actual disk contact, but the shadow is oriented properly to achieve shadow contact. As Pluto passes through opposition, the separation decreases and events involving the disks are again allowed. The model predicts that the mutual-event series ends completely with the superior event of 3 November 1990, though events observable from Earth will cease by mid-August 1990.

VII. CONCLUSIONS

We have presented two approaches to the modeling of Pluto-Charon mutual eclipse event phenomena. The numerical approach is a straightforward, but computationally intensive, discrete-element algorithm. The analytical approach uses the conceptually simple model of three circular disks to represent the planet, satellite, and shadow, and computes the complex geometric relationship among these three disks to obtain the eclipse magnitude at each time step. The results of the two models agree to well within the expected light-curve measurement error.

In the analysis of light-curve observations, the analytic model is to be preferred in the early stages due to its greater speed, for rapid initial optimization of the system parameters in a predictor-corrector scheme (to be discussed and developed in a future paper). The numerical model is capable of a more detailed analysis suitable for fitting limb darkening, albedo features, and other nonuniform parameters as the model becomes better defined and greater complexity is added. The latter will become possible only after initial corrections are made and as additional observational data become available. We have shown, however, that the model is already becoming fairly well constrained by the relatively few observations already obtained.

The authors would like to thank R. P. Binzel, R. M. Nelson, D. J. Tholen, and D. L. Matson for their careful reviews of the original draft of this paper and their helpful suggestions for its revision. The research described in this paper was conducted at the Jet Propulsion Laboratory, California Institute of Technology, under contract with the National Aeronautics and Space Administration.

APPENDIX

We list here the orbit-projection formulas of the Wijesinghe-Tedesco binary light-curve model which are used to set up the analytical-model light-curve computation, supplementing the derivation of the model in Sec. V. The equation numbers in parentheses denote the original numbers from the Icarus paper (Wijesinghe and Tedesco 1979), while the order of presentation reflects the actual computation sequence. The point of departure of the three-circle method from the original model is noted in the text. Corrections that have been made to the original formulas are noted, as well as a few new ones introduced here, to fix typographical and/or mathematical errors in the 1979 paper. The notation is the same as that used in the present paper.

Impact parameter:

$$A_0 = C \sin \psi \qquad (18.0)$$

Some auxiliary angles in the projection:

$$\cos \psi' = \cos \psi \cos \delta \qquad (15.0)$$

$\sin \gamma' = \sin \delta / \sin \gamma'$ (new)
$\sin \gamma = \cos \psi \sin \gamma'$ (16.0 corrected)
The center-to-center projected radius and position angle:
$L/R = C(\sin^2 \theta + \cos^2 \theta \sin^2 \psi)^{1/2}$ (11)
$\cos(\varphi - \delta) = C \sin \theta (L/R) = (d/L) \sin \theta$ (14.2 corrected)
Some quantities needed to compute the shadow disk offset h:
$\tan(\theta' + \gamma) = \sec \psi' \tan(\theta + \gamma')$ (13.2 corrected)
$C' = d'/R = C \cos \theta / \cos \theta', \quad (\psi = 0)$ (12.2 limit)
$= C \sin(\theta + \gamma') / \sin(\theta' + \gamma)$ (12.2 corrected)
$h/R = \tan \alpha (C' - B_0) \cos \theta'$ superior (8.1 modified)
$h/R = \tan \alpha (C' - 1) \cos \theta$ inferior (8.2 modified)
The projected radius and position angle of the shadow disk center:
$L'/L = [1 + (h/L)^2 - 2(h/L) \cos \varphi]^{1/2}$ (7.2 modified)
$\cos \varphi' = (L/L') \cos \varphi - h/L'$ (6.2)

REFERENCES

Andersson, L. E. (1978). Bull. Am. Astron. Soc. **10**, 586.
Binzel, R. P., Tholen, D. J., Tedesco, E. F., Buratti, B., and Nelson, R. M. (1985). Science **228**, 1193.
Bonneau, D., and Foy, R. (1980). Astron. Astrophys. **92**, L1.
Buratti, B. J. (1984). Icarus **59**, 392.
Christy, J. W., and Harrington, R. S. (1978). Astron. J. **83**, 1005.
Harrington, R. S., and Christy, J. W. (1981). Astron. J. **86**, 442.
Hege, E. K., Hubbard, E. N., Drummond, J. D., Strittmatter, P. A., Worden, S. P., and Lauer, T. (1982). Icarus **50**, 72.
Lebofsky, L. A., Rieke, G. H., and Lebofsky, M. J. (1982). Bull. Am. Astron. Soc. **14**, 766.
Mulholland, J. D., and Binzel, R. P. (1984). Astron. J. **89**, 882.
Tholen, D. J. (1985). Astron. J. **90**, 2353.
Walker, A. R. (1980). Mon. Not. R. Astron. Soc. **192**, 47P.
Wijesinghe, M. P., and Tedesco, E. F. (1979). Icarus **40**, 383.